FAST IMAGE CHARGE CALCULATIONS FOR MULTIPARTICLE SIMULATIONS IN FT-ICR ANALYZER CELLS OF ARBITRARY GEOMETRY

SUBMITTED TO Int. J. Mass Spectrom.

Joshua A. Driver[1], Andriy Kharchenko[1,2], Ron M. A. Heeren[2], I. Jonathan Amster[1]

[1]University of Georgia, Department of Chemistry, Athens, GA 30602

[2]FOM Institute AMOLF, Science Park 104, 1098 XG Amsterdam, The Netherlands

***** Address for correspondence

Department of Chemistry, University of Georgia

Athens, Georgia 30602

Phone: (706) 542-2726

FAX: (706) 542-9454

Email: jamster@uga.edu

ABSTRACT

As improvements in Fourier transform ion cyclotron resonance (FT-ICR) mass analyzers continue to provide higher resolving power and better mass accuracy, it becomes important to consider small perturbations to the observed frequency such as those resulting from the interaction between an ion and its image charge. Multi-particle simulations can help in understanding these forces. Previously, particle-in-cell simulations have used a basic implementation of the image charge force on the flat edges of the workspace. In the case of cylindrical cells, however, this does not provide an accurate representation of these forces. Until recently, the calculation of image charge on curved electrodes has been impractical due to the high computational cost, but this cost can be mitigated by parallelizing the calculations on general purpose Graphic Processing Units (GPUs). In this paper, a new parallelizable charge collocation based method for including high resolution image charge effects on surfaces of arbitrary geometry is presented. This method is then used to explore the effects of image charge interactions on observed cyclotron frequency in cylindrical ICR analyzer cells by simulating the trajectories of populations of Cs^+ ranging from 20,000 ions to 1,000,000 ions.

INTRODUCTION

Multi-particle simulations provide a useful approach for studying collective ion motion in an FTICR analyzer cell, and to accurately model the influence of subtle effects such as space-charge and ion-image charge interactions [1-5]. Simulations provide the ability to test the effects of parameters that are difficult to control experimentally such as the precise number and spatial distribution of ions in an analyzer cell [6]. The design of high-performance Fourier transform mass analyzers can be assisted by multiparticle simulations, which can predict the improvements in coherence of ion motion, mass resolving power, and mass accuracy resulting from novel cell designs [7]. Accurate simulation of ion dynamics requires an accounting of subtle effects such as the force introduced by the image charge upon ions moving in the trap. Until recently, modeling precise image charge behavior (i.e. with a sufficiently large number of surface charges) in cells of arbitrary geometry was impractical due to the significantly increased amount of computation time required by existing surface charge calculation methods [1]. However, recent progress in massively parallel coprocessors has made it possible to significantly speed-up such calculations.

To track each ion's evolution in time, we need to integrate the force equation:

$$m\frac{d\boldsymbol{v}}{dt} = q[\boldsymbol{v}\times\boldsymbol{B}] + q\boldsymbol{E}(\boldsymbol{r},t) \quad (1)$$

to find the ion's velocity vector ***v*** where *q* is the charge on the ion, ***B*** is the magnetic field acting on the ion, ***E*** is the composition of electric fields acting on the ion, ***r*** is ion's coordinate vector, *P* is the number of other ions, *m* is ion's mass, and t is the time step. The largest force is due to the magnetic field, and is given by $q[v \times B]$. This force produces cyclotron motion, which in the absence of electric fields, has a frequency given by:

$$\omega_c = \frac{\mathrm{qB}}{\mathrm{m}} \qquad (2)$$

The second term, qE comprises the forces due to electric fields [8, 9].

$$E = E_{app} + E_{sc} + E_{ic} \quad (3)$$

Here $\boldsymbol{E_{app}}$ is the applied electric field created by voltages that are applied to cell electrodes, $\boldsymbol{E_{sc}}$ is the electric field due to ion-ion interactions, also known as space-charge, $\boldsymbol{E_{ic}}$ is the electric field from the image charge induced on the analyzer cell plates. E_{app} is the strongest of the electric fields, while E_{ic} is the weakest.

$\boldsymbol{E_{app}}$ includes both trapping (quadrupolar) and excitation (dipolar) electric fields. Ideally, the ratio of E/r is constant for the trapping potential (r is radial displacement from the central axis of the analyzer cell). The radially repulsive force of the trapping potential leads to magnetron motion of the ion, and a reduction in the observed orbital frequency from the ideal value given by equation 2. For most commonly used analyzer cells, there is a spatial gradient in the trapping field, leading to a change in magnetron frequency across the analyzer cell, and thus, a loss of coherence as ions undergo axial motion [8]. However, the development of harmonized analyzer cells has improved this undesirable behavior [7, 10-13]; magnetron

frequency is very close to a constant over the volume of such compensated analyzer cells. One of the advantages of harmonized cells is their ability to maintain cloud coherence at a higher radius of excitation where space charge effects are less prominent due to the decrease in ion density. However, an increase in excitation radius leads to an increase in the effects of image charge interactions [5]. This means it is necessary to find a compromise between these effects in order to optimize FTICR performance. As mass accuracy continues to improve due to advances in controlling the adverse effects of applied electric fields and space charge on ion motion, smaller effects like image charge can now play a significant role. It would be advantageous to have a better understanding of the magnitude of image charge effects and how they vary due to changes in various parameters.

Next in magnitude are the effects of space charge $\boldsymbol{E_{sc}}$, specifically ion-ion interaction [14, 15]. This perturbation of ion motion can be treated in a global fashion and acts on all ions in a similar manner. Developments such as automated gain control [16] and external calibration functions [17-21] that account for space charge have thoroughly reduced their effects on mass accuracy to the point where other smaller perturbations can be considered. The implementation difficulty comes from the number of calculations, which grows with the number of ions. There are a number of frameworks circumventing this problem and the particle-in-cell (PIC) method, borrowed from the plasma physics community, offers a computationally tractable way to examine motion of realistic numbers of ions while maintaining an accurate account of space charge [22-24]. It avoids the need for calculating $N^2/2$ pairwise forces between N different ions. Instead, the PIC method determines the charge density at each node of a computational mesh, then using this charge density to determine the

forces acting on each ion. The number of such calculations scales with N using the PIC approach, rather than N^2 for the particle-particle approach, greatly reducing the computational effort when modeling the behavior of large populations of ions.

Even smaller in magnitude than space-charge interactions are image-charge interactions with ions $\boldsymbol{E_{ic}}$. Previously, attempts have been made to isolate the effects of ion-image charge interactions [5]. These experiments showed that populations of Cs^+ ions interacted with their image charge to cause a frequency shift that increases in magnitude with ion number and excitation radius. However, these attempts were based on a cubic analyzer cell and used only the basic implementation of image charge interactions provided by PIC calculations in which image charge is calculated on the walls of the orthorhombic PIC grid and included in the $qE(r,t)$ term. The PIC approach calculates the electric field of the trapped ions at each PIC node in the workspace. The electric field at the extents of the cubic workspace is equivalent to image charge, and aligns with the electrode surfaces in a cubic cell simulation, as shown in Figure 1 (left). For a cylindrical cell simulation in a cubic workspace, the location of the image charge force on the flat edges of the workspace is a poor representation of the actual image charge which should accumulate on the cylindrical cell surfaces. To examine these effects in cells with newer cylindrical geometries, more accurate results require the calculation of the image charge on the inner surface of the cylindrical electrodes rather than on the edges of the PIC workspace.

Prior attempts to implement high-resolution image charge simulations experienced performance difficulties due to the need to perform linear algebra operations or even solve the

Poisson equation. The capacitance matrix method, for example, has been used to calculate image charge on cylindrical cells [1], but it cannot be parallelized, and therefore is highly inefficient for simulations of transients of even nominal length. The challenge of making accurate calculations of the image charge created in an arbitrary shaped electrode can be solved by allocating a number of virtual charges on the electrode surface. Then the detected signal is the current of charges between the halves of the outer electrode:

$$\mathrm{I(t)} = \frac{\mathrm{dQ_{1,2}}}{dt} \quad (4)$$

where $Q_{1,2} = Q_1 - Q_2$ is the difference of total surface charges on detection electrodes "1" and "2": $Q_{1,2} = \sum_{i=1}^{N} \sigma_{1,2i}$. This approach, called charge collocation, has the advantage that it can be implemented as parallelizable computer code that can executed using graphical processing units for processing quickly and efficiently. This paper demonstrates this approach, validates by comparison with earlier, slower methods, and applies it to the examination of image charge effects on mass accuracy in a compensated analyzer cell.

EXPERIMENTAL

Multi-particle simulations were performed on Linux clusters at the University of Georgia and the Foundation for Fundamental Research on Matter-Institute for Atomic and Molecular Physics (FOM-AMOLF). Data analysis was performed with FOM-AMOLF's AWE and A. Kharchenko's ParticleVis software. The parameters for the simulations are summarized in Table 1. The analyzer cell geometry is in accordance with a Tolmachev cell design with a diameter of 6

cm. Simulations utilized an idealized quadrupolar trapping potential or a trapping potential defined by a SIMION model of a Tolmachev cell. A monoisotopic population of Cs^+ ions (m/z = 139.905) was generated in a Gaussian distribution along an ellipsoid (major axis = 20 mm; minor axis = 5 mm) with the major axis parallel to the magnetic field. The initial particle velocity distribution is Maxwellian at 300K and the direction of the velocity vector is randomized. For excitation, an on-resonance radiofrequency burst is used at excite voltages between 40 and 320 $V_{p\text{-}p}$ in order to achieve excite radii between 10% and 80% of the cell radius. A simulated time domain transient was collected for each experiment and a frequency domain spectrum was derived using FOM-AMOLF's AWE software [25]. The ion cloud and the resulting image charge distribution was visualized with in-house software developed at FOM-AMOLF [2].

Calculating the surface charge distribution

Let the surface charges having charge density $\rho(x, y, z)$, where x, y, z are Cartesian coordinates, be located in some volume V. If V is bounded, say with a conductor surface S, the Laplace equation $\nabla^2\varphi = 0$ in such a volume will be

$$\frac{1}{4\pi\varepsilon\varepsilon_0}\int_V \frac{\rho}{r}dV = \varphi \quad (5)$$

where r is distance between the integration and observation points. In the case where the charge is located on some surface, for some points A and B on that surface the equation (5) can be reformulated as

$$\frac{1}{4\pi\varepsilon\varepsilon_0}\int_S \frac{\sigma_A}{r_{AB}}dS_A = \varphi_B \quad (6)$$

where S is the conductor surface, σ_A is the surface charge density at location A, dS_A – element of surface at location A, r_{AB} – distance between the points, and φ_B – potential at point B.

If we allocate a grid of N discrete points on the surface S, not necessarily regularly spaced, charge density of each element is constant ($\sigma_i = const$), then equation (6) will become

$$\frac{1}{4\pi\varepsilon\varepsilon_0}\sum_{i=1}^{N}\int_{S_i}\frac{\sigma_i}{r_i}dS_i = \frac{1}{4\pi\varepsilon\varepsilon_0}\sum_{i=1}^{N}\sigma_i\int_{S_i}\frac{dS_i}{r_i} = \varphi_B \quad (7)$$

Such a substitution of a surface integral with a sum of integrals of the surface's elements allows one to find surface charge densities at discrete locations by solving the corresponding system of linear equations with N unknowns σ_i and N coefficients $a_{ij} = \int_{S_i}\frac{dS_i}{r_{ij}}$:

$$\begin{pmatrix} a_{11} & a_{12} & \dots & a_{1n} \\ a_{21} & \ddots & & \vdots \\ \vdots & & \ddots & \vdots \\ a_{n1} & a_{n2} & \dots & a_{nn} \end{pmatrix} \begin{pmatrix} \sigma_1 \\ \vdots \\ \vdots \\ \sigma_n \end{pmatrix} = 4\pi\varepsilon\varepsilon_0 \begin{pmatrix} \varphi_1 \\ \vdots \\ \varphi_n \end{pmatrix} \quad (8)$$

Getting back to the mass spectrometry theme, remember that in an ion trap, surface charges are distributed in a certain way not only under the influence of potentials φ_i but mainly influenced by the ions $q_1 \dots q_P$, each at a distance d_{ik}, whose field can be approximated by the point charge potential $\varphi_Q = \frac{q_i}{4\pi\varepsilon\varepsilon_0 d_i}$. Accordingly, equations (7) and (8) should be reformulated as

$$\sum_{i=1}^{N} \sigma_i \int_{S_i} \frac{dS_i}{r_i} = \frac{1}{4\pi\varepsilon\varepsilon_0} \left(\varphi_B - \sum_{k=1}^{P} \frac{q_k}{d_{ik}} \right)$$

and

$$\begin{pmatrix} a_{11} & a_{12} & \dots & a_{1n} \\ a_{21} & \ddots & & \vdots \\ \vdots & & \ddots & \vdots \\ a_{n1} & a_{n2} & \dots & a_{nn} \end{pmatrix} \begin{pmatrix} \sigma_1 \\ \vdots \\ \vdots \\ \sigma_n \end{pmatrix} = 4\pi\varepsilon\varepsilon_0 \begin{pmatrix} \varphi_1 - \sum_{k=1}^{P} \frac{q_k}{d_{1k}} \\ \vdots \\ \varphi_n - \sum_{k=1}^{P} \frac{q_k}{d_{nk}} \end{pmatrix} \quad (9)$$

where d_{ik} is a distance between the k-th ion and i-th surface charge location. The negative sign of the sums of ions' potentials is explained by the opposite charges of the ions and surface charges that they induce. At $i \quad j$ coefficient a_{ij} is finite, but it has a singularity at $i = j$, however, the expression is integrable: if we consider a disc of small radius R around point i, then remembering that $dS = rdrd\alpha$, we can state that

$$\int_{S_i} \frac{dS_i}{r_{ij}} = \int_0^{2\pi} \int_0^R \frac{r dr}{r_{ij}} d\alpha = 2\pi R \quad (10)$$

which proves that a_{ij} is finite at both $i \quad j$ and $i = j$. Figure 9 demonstrates how this is applied to the electrode surface of an FTICR mass analyzer.

A more detailed description of the PIC method and how it incorporates charge collocation can be found in the Supplemental Data.

Remark on the capacitance matrix approach

Matrix

$$A = \begin{pmatrix} a_{11} & a_{12} & \dots & a_{1n} \\ a_{21} & \ddots & & \vdots \\ \vdots & & \ddots & \vdots \\ a_{n1} & a_{n2} & \dots & a_{nn} \end{pmatrix} \quad (11)$$

in equation 9 can also be considered as the Maxwell capacitance matrix C of a system of conductors having voltages V and charges Q:

$$Q = C\,V \quad (12)$$

This suggests an alternative method of calculating elements of *A*: to calculate the k-th column one should set the potential of k-th conductor (that is, k-th element of V) to 1 leaving the other conductors' potentials equal to 0 and the resulting vector of Q will yield the k-th column of C. As a result we have a system of N equations for N unknowns which determines values of the surface charges induced on each electrode. It can be numerically solved via pseudo-inversion.

This method has been used previously to study space charge in an orbitrap FTMS analyzer [1, 3], however, it is not parallelizable and thus requires a large amount of computational time.

RESULTS AND DISCUSSION

Method validation and stability

To determine the number of image charge points necessary for stability, simulations were performed with increasing density of surface charges and the observed frequency was monitored, as shown in Figure 3a. With very few surface charges, the frequency varies as much as 0.35 Hz with surface charge density. Once a sufficient number of surface charges are used, the frequency is stable. Figure 3a shows that the observed shifts will be reproducible if the number of surface charges is greater than about 4 per square cm of conductor surface.

To make sure the charge collocation method returned accurate results, it was necessary to make a comparison with an established method. The simplest way of doing this was to compare directly to the previous particle in cell method for determining image charge shifts in a cubic cell. Surface charges were placed equidistant along the boundaries of the workspace for a 2 in cubic cell. This effectively mimics the previous PIC method of calculating image charge forces on the rectilinear boundaries of the workspace [24]. At first, this setup resulted in frequency shifts approximately twice that of the original PIC method. It became apparent then that we had to remove the boundary PIC points from the force equation in order to not have the image charge force applied from both the PIC calculation and the charge collocation method. This removal of points becomes especially important for application of this method to cylindrical cells because without this extra step the image charge force on the ions would be

the force from the edges of the workspace superimposed upon that of the cylindrical electrodes. Figure 3b shows the observed frequency shifts vs. increasing excitation radius for both the charge collocation method and the PIC method. The average difference between these two methods is 2.6 mHz or a relative error of 3.2 ppb. The simulations show a shift of 2.0×10^{-6} Hz per ion in a 5 cm (2 inch) cubic cell at 7.0 T, due to the interaction of an ion with its image charge. Several groups have previously made analytical calculations of image charge force for a single ion, which we can use as a baseline for comparison [26, 27]. Marshall and coworkers calculated the force in a 2.5 cm cubic cell at 3.0 T to be 1.0×10^{-5} Hz per ion for excitation to 50% of the cell radius. Correcting for the 1/B dependence, this shift becomes 4.6×10^{-6} Hz per ion at 7.0 T. Tinkle and Barlow calculated the shift in a 4 cm cubic cell at 7.0 T to be 2.7×10^{-6} Hz per ion. Given the differences in cell design and initial ion locations, our simulations are in good agreement with these analytically derived values. We can also consider a comparison to experimental results as additional evidence of this method's validity. Even though we cannot accurately determine the number of ions in the analyzer cell during an experiment, we can check that the observed frequency shift corresponds to a reasonable number of ions. Wong et al. have measured a cyclotron frequency shift as a function of Cs^+ ion intensity, with a 50 fold difference in ion intensity between the highest and lowest ion numbers used in this experiment [28]. The frequency shift between the largest and smallest population of ions is 0.7 Hz, roughly corresponding to 350000 ions, using the PIC derived value for frequency shift per ion of 2.0×10^{-6} Hz. This number of ions seems reasonable for a high intensity peak, and suggests agreement with the PIC calculated value for image-charge induced frequency shift.

Implementation and performance

An incentive to use the charge collocation method, albeit its computational cost, is its intrinsic parallelism allowing an efficient implementation on a computation cluster of the multiple-instruction multiple-data (MIMD) type. Being performed on independent processing units, equation 9, apart from parallelism, require accessing a large number of adjacent memory locations (the arrays of ion charge and position) which motivated our choice of Graphics Processing Units (GPUs) hardware of the single-instruction multiple-data (SIMD) type, known to excel in computational schemes with coalesced memory access. Figure 4 presents graphical examples of charge collocation method solutions performed on a NVidia Tesla K2. The images represent snapshots of the image charge and ion distribution for simulations of 100,000 singly charged ions (m/z 133) undergoing cyclotron motion in an open-ended cylindrical cell and a cubic cell. The optimized parallel structuring of the calculations greatly decreases the computation time for each integration step. This reduction in computation time becomes even more significant as the number of surface charges and the number of ions increases, as shown in Figure 5. A comparison of performance of the detection signal simulation on a GPU (Figure 5a) versus a conventional computer architecture (Figure 5b) shows a speedup of over two orders of magnitude. The speedup is independent of the number of surface charges or the number of ions in the simulation, as shown in Figure 5c.

Analysis of Image Charge Effects in a Harmonized Cylindrical Cell

The principal utility of the collocation method for image charge calculations is its ability to be readily applied to analyzer cells of arbitrary geometry. We have applied this approach to investigate the performance of a compensated cylindrical cell based on the design of Tolmachev [12]. In order to examine only the effects of image charge, simulations were performed with a single mass-to-charge value of 132.905 corresponding to the Cs^+ ion. By using ions of a single mass-to-charge, conventional ion-ion space charge shifts to cyclotron frequency are eliminated, and only image charge shifts will be observed [5]. Figure 6 shows the observed frequency of simulated populations of ions at different radii of excitation in an ideal 3D hyperbolic trapping field. The results show a frequency shift that increases as the ions go to higher radius by a factor of $1/d^2$ as would be expected for two point charges. Additionally, the frequency shift grows with increasing numbers of ions, due to their higher charge density creating a larger image potential on the electrode surface. For 100k ions of the same mass-to-charge, there is an ~ 80 ppb shift in frequency from detection at 10% of the cell radius and detection at 80% of the cell radius with most of this shift occurring at higher radii. This shift becomes ~ 120 ppb with 500k ions. This is problematic since one goal of many harmonized analyzer cells is to be able to utilize higher radius excitation to mitigate frequency shifts due to traditional space charge.

For the Tolmachev cell design, the results become more complex. Because there can only be a finite number of shimming electrodes (in this case 4) the resulting trapping field cannot be perfectly quadrupolar. There are small perturbations in the electric field that cause the observed frequency to deviate even without image charge forces taken into account. This is

normally a detriment to the Tolmachev design, since the anharmonicity of the cell leads to quicker ion cloud destruction. In this case, however, these frequency shifts run counter to those caused by image charge and compensate for the image charge forces to a small degree. Figure 7 shows that this effect is most notable at ~ 100k ions as the anharmonic terms of the electric field and the force from image charge nearly cancel each other out giving a very small (~ 50 ppb) change from excitation of 50% to 80% of the cell radius. These small perturbations in the electric field are a constant effect, and with higher numbers of ions can be overwhelmed to create a situation that looks very similar to the ideal electric field radial dependence.

Considerations for Mass Calibration and Cell Design

In the case of mass spectra in which the distribution of intensities is relatively uniform and ions are excited to the same radius, image charge effects will be negligibly small. There are, however, several cases where this is not possible. Certain MS/MS methods with low conversion efficiency, such as electron capture dissociation [29] or electron detachment dissociation [30], result in a very intense precursor, but product ion peaks of relatively low intensity. In this case the frequency shift due to image charge will be higher for the precursor than for the products and as a result the precursor should not be used for internal or lock-mass calibration. For example, assuming a precursor consisting of 500,000 ions where the products are approximately 5 percent of the parent, the shift for the parent ion due to image charge would be 1.3 ppm and the shift for the products would be 60 ppb at 7 T. At higher magnetic fields this problem is alleviated somewhat; at 15 T the shift on the parent would be 0.5 ppm and the product would be 30 ppb. Additionally, image charge forces should be taken into account when

calibrating spectra in which ions are excited to different radii as in the case of 2D FTICR/MS [31]or to reduce the effects of conventional ion-ion space charge [32].

In terms of cell design, image charge creates the transient and so cannot be completely eliminated. We can however limit the effect it has on the observed frequency. One of the biggest contributors to image charge force is the ion charge density. The Tolmachev cell design only holds ions in the space inside the compensated area of the cell. The ideal electric field is compensated over the entire space and therefore there is more room for ions to spread out along the z-axis, decreasing ion charge density and, as a result, image charge force. This advantage can be applied to real cells that utilize the entirety of the cell to hold ions, such as the Boldin-Nikolaev [7] and the externally shimmed 'window' cell [33].

CONCLUSIONS

Particle-in-cell ion trajectory calculations provide the means to gain insight into the fundamentals of ion behavior in FTICR-MS. An extended PIC algorithm for arbitrary electrode surfaces high-resolution image charge calculation has been implemented on CUDA-compliant graphical processors and is being run on a range of graphical cards: Nvidia Tesla C1070, C2070, and K20. The charge collocation method allows modeling real ICR cells' performance in critical regimes of interaction with the image charge (e.g. high excitation radius, large ion population) in a reasonable time frame via the inherent parallelizability of the method.

ACKNOWLEDGEMENTS

The authors acknowledge the generous support of the National Science Foundation, grants CHE-1058913 and OISE-0730072.

REFERENCES

[1] E.N. Nikolaev, Y.I. Kostyukevich, G.N. Vladimirov, Fourier transform ion cyclotron resonance (FT ICR) mass spectrometry: Theory and simulations, Mass spectrometry reviews, (2014) in press.
[2] W. Burakiewicz, R. van Liere, Analyzing complex FTMS simulations: A case study in high-level visualization of ion motions, Ieee Transactions on Visualization and Computer Graphics, 12 (2006) 1037-1043.
[3] A. Kharchenko, G. Vladimirov, R.M.A. Heeren, E.N. Nikolaev, Performance of Orbitrap Mass Analyzer at Various Space Charge and Non-Ideal Field Conditions: Simulation Approach, J Am Soc Mass Spectr, 23 (2012) 977-987.
[4] F.E. Leach, A. Kharchenko, G. Vladimirov, K. Aizikov, P.B. O'Connor, E. Nikolaev, R.M.A. Heeren, I.J. Amster, Analysis of phase dependent frequency shifts in simulated FTMS transients using the filter diagonalization method, Int J Mass Spectrom, 325 (2012) 19-24.
[5] F.E. Leach, A. Kharchenko, R.M.A. Heeren, E. Nikolaev, I.J. Amster, Comparison of Particle-In-Cell Simulations with Experimentally Observed Frequency Shifts Between Ions of the Same Mass-To-Charge in Fourier Transform Ion Cyclotron Resonance Mass Spectrometry, J Am Soc Mass Spectr, 21 (2010) 203-208.
[6] G. Vladimirov, C.L. Hendrickson, G.T. Blakney, A.G. Marshall, R.M.A. Heeren, E.N. Nikolaev, Fourier Transform Ion Cyclotron Resonance Mass Resolution and Dynamic Range Limits Calculated by Computer Modeling of Ion Cloud Motion, J Am Soc Mass Spectr, 23 (2012) 375-384.
[7] E.N. Nikolaev, I.A. Boldin, R. Jertz, G. Baykut, Initial experimental characterization of a new ultra-high resolution FTICR cell with dynamic harmonization, J Am Soc Mass Spectrom, 22 (2011) 1125-1133.
[8] I.J. Amster, Fourier Transform Mass Spectrometry, Journal of Mass Spectrometry, 31 (1996) 1325-1337.
[9] A.G. Marshall, C.L. Hendrickson, G.S. Jackson, Fourier transform ion cyclotron resonance mass spectrometry: A primer, Mass spectrometry reviews, 17 (1998) 1-35.
[10] A.M. Brustkern, D.L. Rempel, M.L. Gross, An electrically compensated trap designed to eighth order for FT-ICR mass Spectrometry, J Am Soc Mass Spectr, 19 (2008) 1281-1285.
[11] N.K. Kaiser, J.J. Savory, A.M. McKenna, J.P. Quinn, C.L. Hendrickson, A.G. Marshall, Electrically compensated Fourier transform ion cyclotron resonance cell for complex mixture mass analysis, Anal Chem, 83 (2011) 6907-6910.
[12] A.V. Tolmachev, E.W. Robinson, S. Wu, H. Kang, N.M. Lourette, L. Pasa-Tolic, R.D. Smith, Trapped-ion cell with improved DC potential harmonicity for FT-ICR MS, J Am Soc Mass Spectrom, 19 (2008) 586-597.
[13] A.V. Tolmachev, E.W. Robinson, S. Wu, R.D. Smith, L. Pasa-Toli, Trapping radial electric field optimization in compensated FTICR cells, J Am Soc Mass Spectrom, 22 (2011) 1334-1342.
[14] T.J. Francl, M.G. Sherman, R.L. Hunter, M.J. Locke, W.D. Bowers, R.T. Mciver, Experimental-Determination of the Effects of Space-Charge on Ion-Cyclotron Resonance Frequencies, International Journal of Mass Spectrometry and Ion Processes, 54 (1983) 189-199.
[15] J.B. Jeffries, S.E. Barlow, G.H. Dunn, Theory of Space-Charge Shift of Ion-Cyclotron Resonance Frequencies, International Journal of Mass Spectrometry and Ion Processes, 54 (1983) 169-187.
[16] J.E.P. Syka, J.A. Marto, D.L. Bai, S. Horning, M.W. Senko, J.C. Schwartz, B. Ueberheide, B. Garcia, S. Busby, T. Muratore, J. Shabanowitz, D.F. Hunt, Novel linear quadrupole ion trap/FT mass spectrometer: Performance characterization and use in the comparative analysis of histone H3 post-translational modifications, Journal of Proteome Research, 3 (2004) 621-626.

[17] R.L. Wong, I.J. Amster, Sub part-per-million mass accuracy by using stepwise-external calibration in Fourier transform ion cyclotron resonance mass spectrometry, J Am Soc Mass Spectr, 17 (2006) 1681-1691.
[18] D.K. Williams, D.C. Muddiman, Parts-per-billion mass measurement accuracy achieved through the combination of multiple linear regression and automatic gain control in a Fourier transform ion cyclotron resonance mass spectrometer, Analytical Chemistry, 79 (2007) 5058-5063.
[19] D.K. Williams, A.L. Kovach, D.C. Muddiman, K.W. Hanck, Utilizing Artificial Neural Networks in MATLAB to Achieve Parts-Per-Billion Mass Measurement Accuracy with a Fourier Transform Ion Cyclotron Resonance Mass Spectrometer, J Am Soc Mass Spectr, 20 (2009) 1303-1310.
[20] D.K. Williams, M.A. Chadwick, T.I. Williams, D.C. Muddiman, Calibration laws based on multiple linear regression applied to matrix-assisted laser desorption/ionization Fourier transform ion cyclotron resonance mass spectrometry, Journal of Mass Spectrometry, 43 (2008) 1659-1663.
[21] D.C. Muddiman, A.L. Oberg, Statistical evaluation of internal and external mass calibration laws utilized in Fourier transform ion cyclotron resonance mass spectrometry, Analytical Chemistry, 77 (2005) 2406-2414.
[22] C.K. Birdsall, Particle-in-cell charged-particle simulations, plus Monte Carlo collisions with neutral atoms, PIC-MCC, Plasma Science, IEEE Transactions on, 19 (1991) 65-85.
[23] D.W. Mitchell, Realistic simulation of the ion cyclotron resonance mass spectrometer using a distributed three-dimensional particle-in-cell code, J Am Soc Mass Spectr, 10 (1999) 136-152.
[24] D.W. Mitchell, R.D. Smith, Two dimensional many particle simulation of trapped ions, Int J Mass Spectrom, 165 (1997) 271-297.
[25] T.H. Mize, I. Taban, M. Duursma, M. Seynen, M. Konijnenburg, A. Vijftigschild, C.V. Doornik, G.V. Rooij, R.M.A. Heeren, A modular data and control system to improve sensitivity, selectivity, speed of analysis, ease of use, and transient duration in an external source FTICR-MS, Int J Mass Spectrom, 235 (2004) 243-253.
[26] X.Z. Xiang, P.B. Grosshans, A.G. Marshall, Image Charge-Induced Ion-Cyclotron Orbital Frequency-Shift for Orthorhombic and Cylindrical Ft-Icr Ion Traps, International Journal of Mass Spectrometry and Ion Processes, 125 (1993) 33-43.
[27] M.D. Tinkle, S.E. Barlow, Image charge forces inside conducting boundaries, Journal of Applied Physics, 90 (2001) 1612-1624.
[28] R.L. Wong, I.J. Amster, Experimental evidence for space-charge effects between ions of the same mass-to-charge in Fourier-transform ion cyclotron resonance mass spectrometry, Int J Mass Spectrom, 265 (2007) 99-105.
[29] R.A. Zubarev, N.L. Kelleher, F.W. McLafferty, Electron capture dissociation of multiply charged protein cations. A nonergodic process, Journal of the American Chemical Society, 120 (1998) 3265-3266.
[30] J.J. Wolff, I.J. Amster, L.L. Chi, R.J. Linhardt, Electron detachment dissociation of glycosaminoglycan tetrasaccharides, J Am Soc Mass Spectr, 18 (2007) 234-244.
[31] M.A. van Agthoven, M.A. Delsuc, C. Rolando, Two-dimensional FT-ICR/MS with IRMPD as fragmentation mode, Int J Mass Spectrom, 306 (2011) 196-203.
[32] N.K. Kaiser, A.M. McKenna, J.J. Savory, C.L. Hendrickson, A.G. Marshall, Tailored Ion Radius Distribution for Increased Dynamic Range in FT-ICR Mass Analysis of Complex Mixtures, Analytical Chemistry, 85 (2013) 265-272.
[33] A.V. Tolmachev, E.W. Robinson, R.D. Smith, F.E. Leach, J.H. Futrell, L. Pasa-Tolic, A conceptual approach for FT-ICR cell harmonization utilizing external shim electrodes, Int J Mass Spectrom, 325 (2012) 45-50.

Table 1. Parameters utilized for PIC stimulations

Trapping potential	1.0 V
Magnetic field	7.0 T
Analyzer geometry	Tolmachev
Ion cloud	Ellipsoid
Semi-major axis	0.2 cm
Semi-minor axis	0.05 cm
Trap dimensions	6 cm x 6 cm x 175 cm
PIC grid	31 x 31 x 90
Simulated particles	10,000–500,000
Ion *m/z*	132.905
Excitation	
Voltage	40–320 V*p-p*
Excitation steps	4800
Duration	52.8 μs
Time step	0.011 μs/step
Detection	
Detection steps	32000
Duration	0.704 ms
Time step	0.022 μs/step

FIGURE CAPTIONS

Figure 1. (Left) Image charge calculation provided by the PIC method; (right) the desired surface of a real detection electrode where the image charge should be measured.

Figure 2. Principle of surface charge density calculation in the presence of ions in the trap. The grid of surface charges are shown as colored balls, where the color represents charge density (blue is maximum negative charge density, red is maximum positive charge density, with intermediate values following the color scale of the rainbow.) Ions are represented by q_n and q_m. The charge density at a specific node is determined from the charges at surrounding nodes and from ions trapped in the analyzer cell (see supplemental text).

Figure 3. Frequency shift as function of the surface charge grid size and as observed for different methods for calculating image charge. (a) Relative error in observed frequency for increasing number of surface charges in 5 cm cubic cell, determined by comparison of simulation results using the collocation method versus results using the PIC workspace grid. (b) Comparison of image charge induced frequency shifts in the cubic cell for the collocation method for calculating image charge versus using the implicit image charge on the surface of the PIC workspace. These give identical results, as expected for a cubic cell. When the image charge calculation is eliminated in the PIC simulation, the observed cyclotron frequency is constant for all excitation radii, as shown by the green line.

Figure 4. Snapshots of 100K Cs ion cloud with the induced image charge distribution in the Tolmachev (left) and cubic (right) analyzer cells. The charge distribution on the cubic surface is shown without the front XY edge.

Figure 5. Simulation time comparison between GPU and CPU calculations. (a) Performance versus number of surface charges, using a GPU for the image charge calculation. The metric for performance is the duration of one time step (calculating the new position of all ions, and the electric field and image charge distribution). (b) Same calculation as in (a), but using the CPUs of the Linux cluster to perform the image charge calculation. (c) Scalability of the overall simulation time as function of the number of surface charges.

Figure 6. Absolute image charge frequency shifts in an ideal trap field as a function of radius of gyration and number of trapped ions. The orbital frequency from the simulation is shown on the left vertical axis, and a scale in ppb is displayed on the right vertical axis.

Figure 7. Absolute image charge frequency shifts in the trap field of Tolmachev design compensated cell as a function of radius of gyration and number of trapped ions. The orbital frequency from the simulation is shown on the left vertical axis, and a scale in ppb is displayed on the right vertical axis.

Figure 1

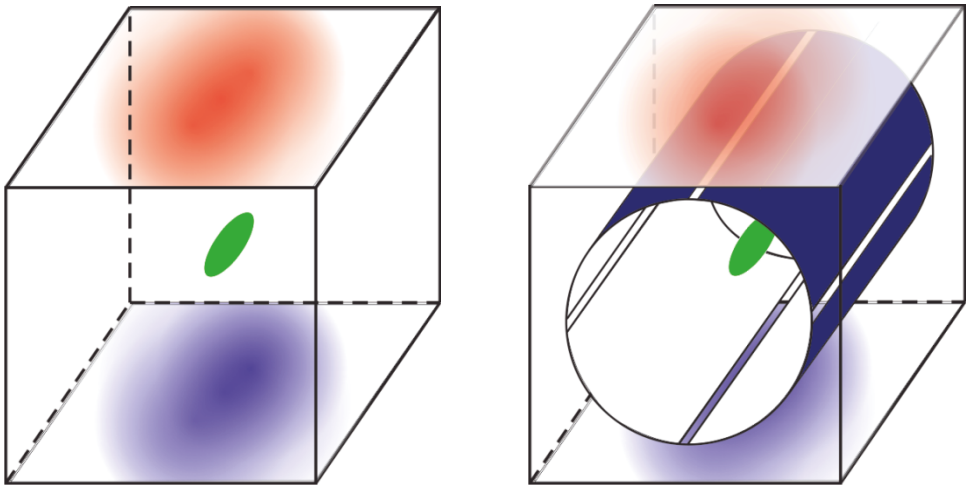

Figure 2

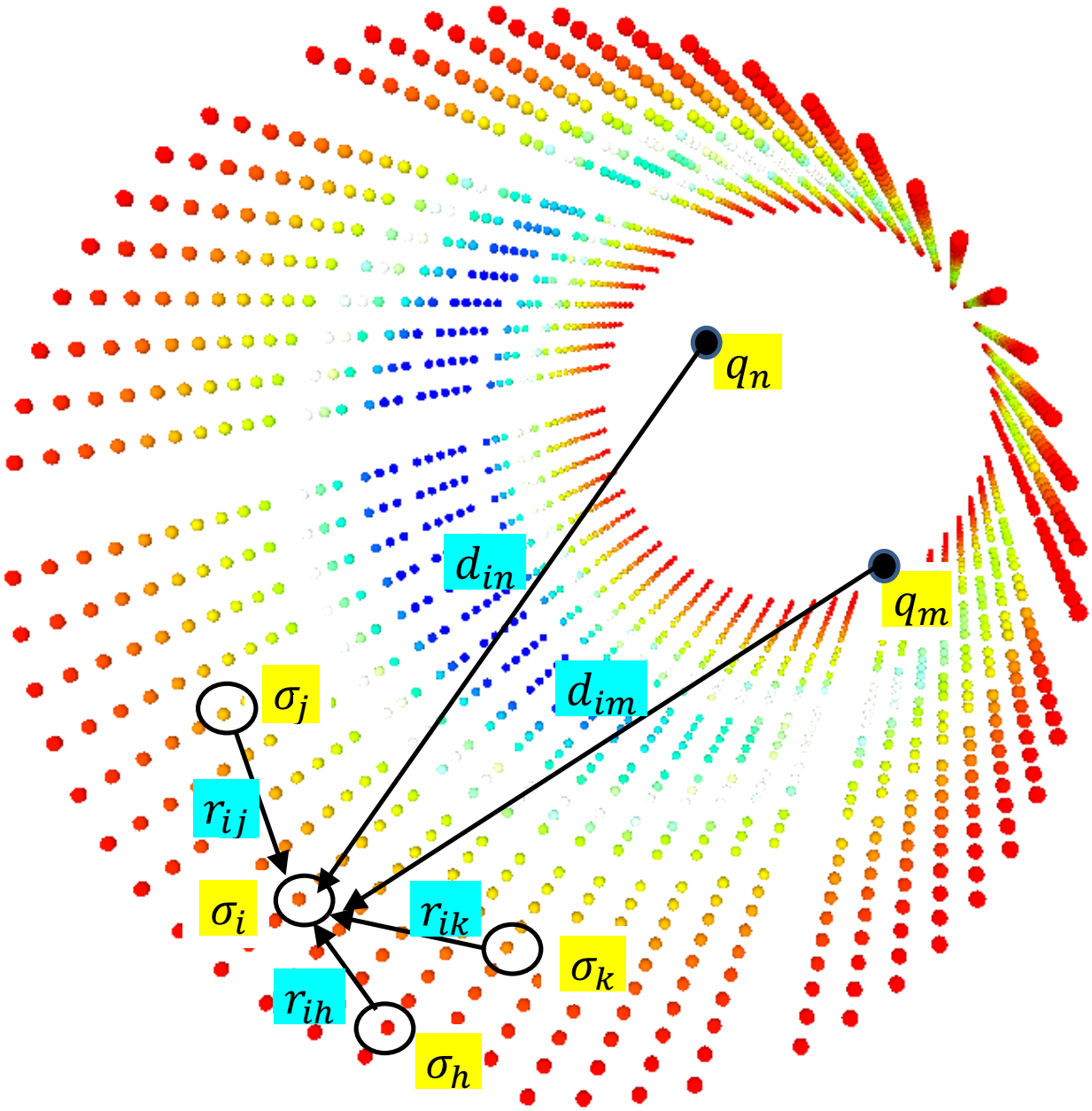

Figure 3

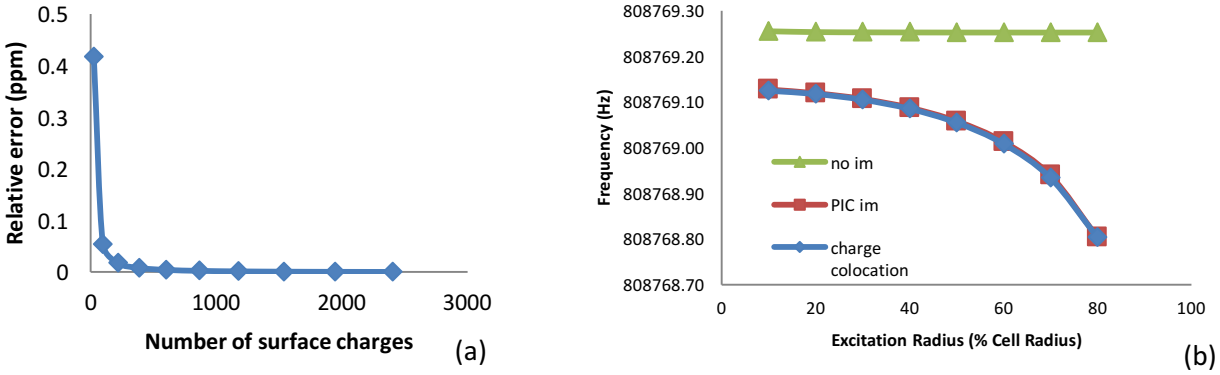
0.5
0.4
0.3
0.2
0.1
0
Relative error (ppm)
0
1000
2000
3000
Number of surface charges
(a)
808769.30
808769.20
808769.10
808769.00
808768.90
808768.80
808768.70
Frequency (Hz)
no im
PIC im
charge colocation
0
20
40
60
80
100
Excitation Radius (% Cell Radius)
(b)

Figure 4

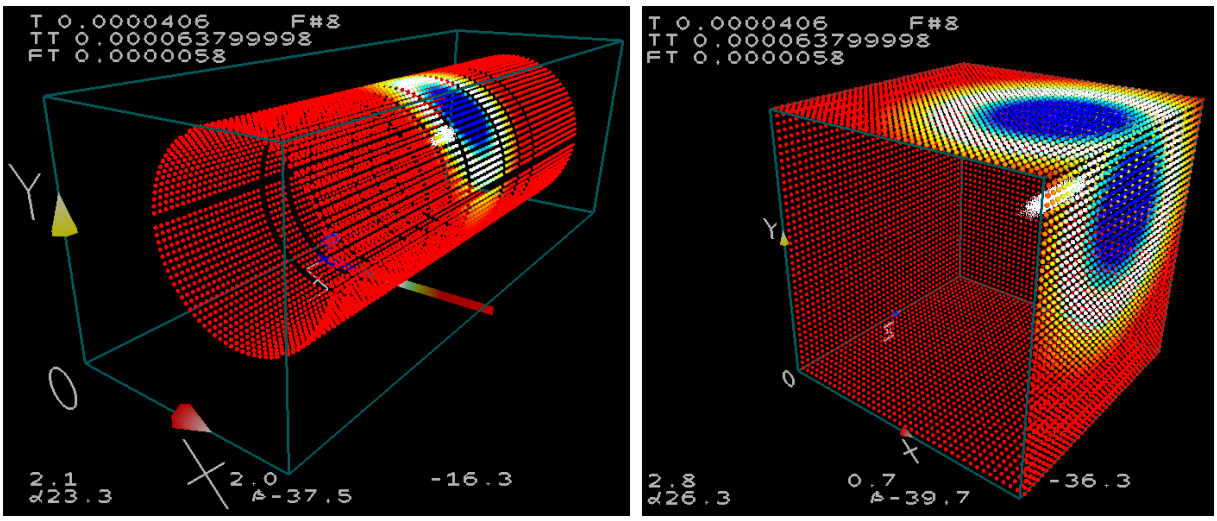
T 0.0000406 F#8
TT 0.000063799998
FT 0.0000058
Y
0
X
2.1
∠23.3
2.0
∠-37.5
-16.3
T 0.0000406 F#8
TT 0.000063799998
FT 0.0000058
Y
0
X
2.8
∠26.3
0.7
∠-39.7
-36.3

(a) (b)

Figure 5

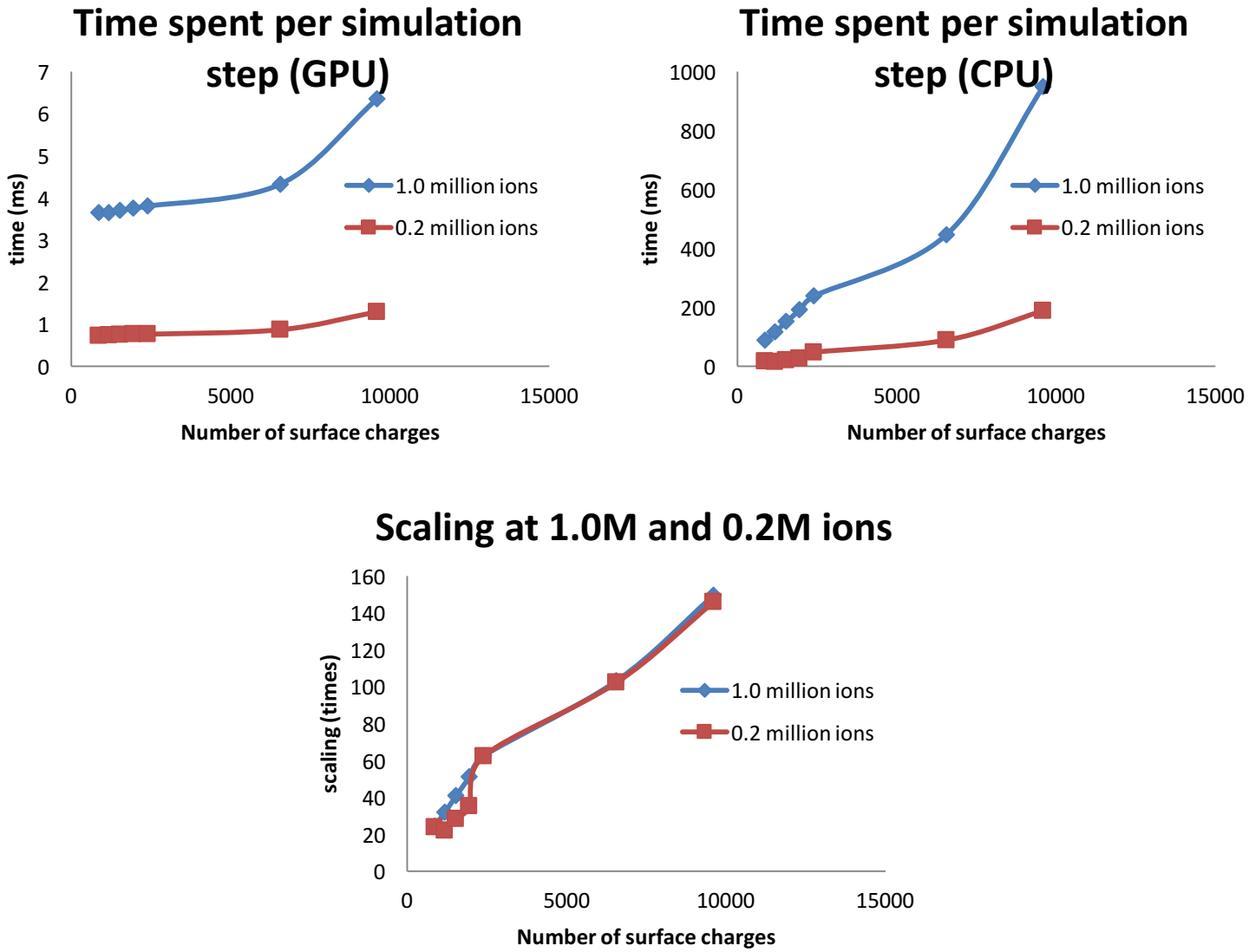
Time spent per simulation step (GPU)
time (ms)
0
1
2
3
4
5
6
7
0
5000
10000
15000
Number of surface charges
1.0 million ions
0.2 million ions
Time spent per simulation step (CPU)
time (ms)
0
200
400
600
800
1000
0
5000
10000
15000
Number of surface charges
1.0 million ions
0.2 million ions
Scaling at 1.0M and 0.2M ions
scaling (times)
0
20
40
60
80
100
120
140
160
0
5000
10000
15000
Number of surface charges
1.0 million ions
0.2 million ions

Figure 6

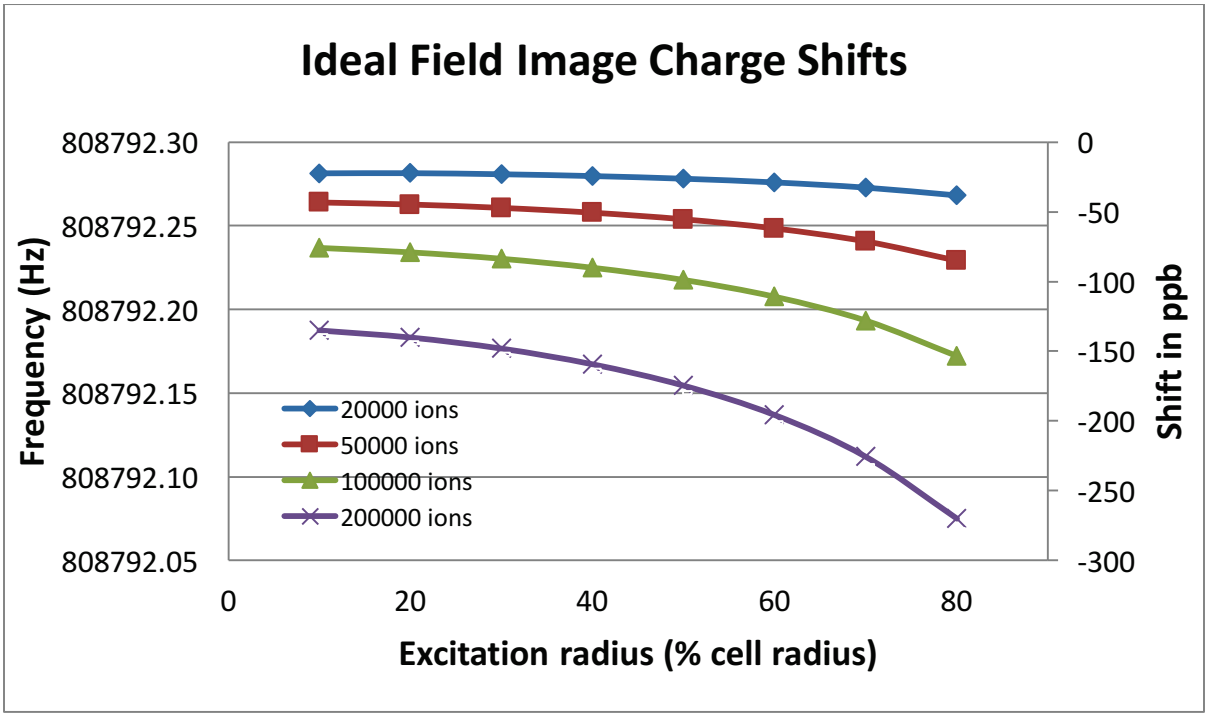
Ideal Field Image Charge Shifts
808792.30
808792.25
808792.20
808792.15
808792.10
808792.05
Frequency (Hz)
0
-50
-100
-150
-200
-250
-300
Shift in ppb
20000 ions
50000 ions
100000 ions
200000 ions
0
20
40
60
80
Excitation radius (% cell radius)

Figure 7

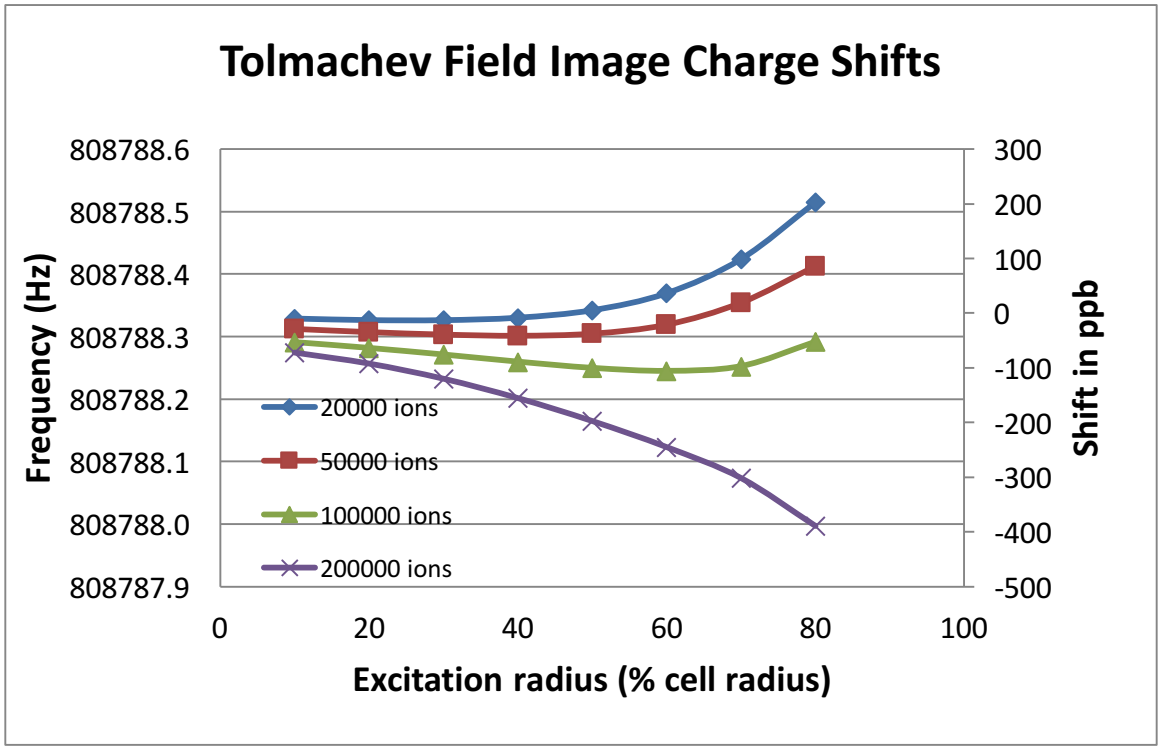
Tolmachev Field Image Charge Shifts
808788.6
808788.5
808788.4
808788.3
808788.2
808788.1
808788.0
808787.9
Frequency (Hz)
300
200
100
0
-100
-200
-300
-400
-500
Shift in ppb
0
20
40
60
80
100
Excitation radius (% cell radius)
20000 ions
50000 ions
100000 ions
200000 ions